Accepted Manuscript

Influence of dimple shape on tribofilm formation and tribological properties of textured surfaces under full and starved lubrication

Yufu Xu, Quan Zheng, Rasha Abuflaha, Dustin Olson, Octavio Furlong, Tao You, Qiangqiang Zhang, Xianguo Hu, Wilfred T. Tysoe

PII: S0301-679X(19)30167-7

DOI: https://doi.org/10.1016/j.triboint.2019.03.047

Reference: JTRI 5689

To appear in: *Tribology International*

Received Date: 7 January 2019

Revised Date: 12 March 2019

Accepted Date: 19 March 2019

Please cite this article as: Xu Y, Zheng Q, Abuflaha R, Olson D, Furlong O, You T, Zhang Q, Hu X, Tysoe WT, Influence of dimple shape on tribofilm formation and tribological properties of textured surfaces under full and starved lubrication, *Tribology International* (2019), doi: https://doi.org/10.1016/j.triboint.2019.03.047.

Influence of dimple shape on tribofilm formation and tribological properties of textured surfaces under full and starved lubrication

Yufu Xu[a*], Quan Zheng[a], Rasha Abuflaha[b,c], Dustin Olson[b], Octavio Furlong[d], Tao You[a], Qiangqiang Zhang[a], Xianguo Hu[a], Wilfred T. Tysoe[b]

a. Institute of Tribology, School of Mechanical Engineering, Hefei University of Technology, Hefei 230009, China

b. Department of Chemistry and Biochemistry and Laboratory for Surface Studies, University of Wisconsin-Milwaukee, Milwaukee 53211, United States

c Department of Chemistry, Al al-Bayt University, P.O. Box 130040, Mafraq 25113, Jordan

d. Physics Department, National University of San Luis, Ejercito de Los Andes 950 -5700, Argentina.

Abstract: Lubrication conditions have significant influences on the formation of tribofilms and then affect tribological behavior. In this work, the influence of tribofilm formation on the tribological behavior of textured surfaces with oval shapes was measured using a pin-on-plate tribometer. The results show that, under full lubrication, the adsorbed oil film controlled the friction and wear behavior of steel/steel tribopairs but under starved lubrication, the formation of a tribofilm significantly influenced the tribological behavior. The appropriate textured surfaces with oval-shaped dimples contributes to obtaining excellent antifriction and antiwear behavior. However, excessively high ratios of the major to the minor axis of the oval can result in high contact stresses which can destroy the tribofilm.

Keywords: Tribofilm; Textured surfaces; Full lubrication; Starved lubrication

* Corresponding author. E-mail: xuyufu@hfut.edu.cn (Y. Xu)

1. Introduction

The control and prediction of friction and wear has become increasingly important with the need for more efficient machines and more advanced manufacturing strategies. Over the last two decades, laser surface texturing has been intensively explored as a means for improving tribological properties [1-3] and has been shown to reduce friction and wear [4-7]. As a consequence, work has focused on understanding the mechanisms by which surface texturing operates [8-13]. However, under some conditions, textured surfaces can also result in higher wear compared to untextured ones [14] and, in many cases, the desired friction and wear performance still cannot be precisely predicted for textured surfaces.

Widely accepted models for the friction and wear reduction of textured surfaces include the formation of micro-reservoirs of the lubricating oil under starved conditions [15] or the presence of micro-traps for wear debris [16]. In addition, the formation of hydrodynamic oil pockets is regarded as beneficial for the lubrication of textured surfaces under full fluid lubrication [17]. Recently, it was also shown that, in addition to these roles, tribofilm formation during sliding can play an important role in the tribological behavior of the textured surfaces [18]. Furthermore, the nature of the lubrication regime can have a significant influence on tribofilm formation [19-21], which ultimately affects the tribological behavior. However, the exact lubrication mechanisms for textured surfaces under different lubrication regimes are still unknown; understanding the influence of texturing on tribofilm formation during sliding is central to understanding the tribological behavior under different lubrication conditions.

Although the shapes of the textured dimples have been shown to significantly affect

tribological behavior in many cases [22-24], there is no uniform view on which texture can provide the optimal tribological properties. In addition, oval-shaped textures have seldom been studied [8]. This is likely to be due to the fact that the most commonly used laser-surface-texturing technology does not easily lend itself to making oval textured surfaces with micro-size. Furthermore, the debris produced by laser texturing requires the sample to be polished after texturing, thereby adding complexity to the process. These issues can be avoided by using the photolithographic etching [18, 25, 26], which affords a facile method for making complex textured surfaces merely by changing the shape of the mask used for defining the etching pattern, and obviates the need for polishing the sample after the textures have been formed. The oval shapes textured surfaces have shown good antifriction and antiwear properties in some cases [27]. However, the lubrication mechanisms of these surfaces under full and starved lubrication have not yet been illustrated. In this work, oval-shaped dimples were prepared by photolithographic etching, and the tribological behavior was investigated under both full and starved lubrication and their tribological properties and the resulting nature of the tribofilms were investigated.

2. Experimental

2.1 Tribological tests

The friction and wear tests were carried out on a pin-on-plate tribometer under the reciprocating motion as shown in **Fig. 1**. Based on the previous literatures [17, 28-30] for the fully lubricated condition, the lubricating oil was supplied dropwise into the contact zone at a rate of 1×10^{-4} dm^3/min, and the interval of the oil drops was 20s. To create starved-lubrication

conditions, only two oil drops were added to contact zone at the beginning of the test, after which no further lubricant was added. The detailed test conditions are listed in **Table 1**. The experiments under each condition were repeated twice and the friction coefficient was continuously recorded by the instrument. The wear volume was calculated by multiplying the cross-sectional area of the wear track by the stroke length. The cross-sectional area was calculated from the base line and the profile which was perpendicular to the sliding direction and did not pass the dimples.

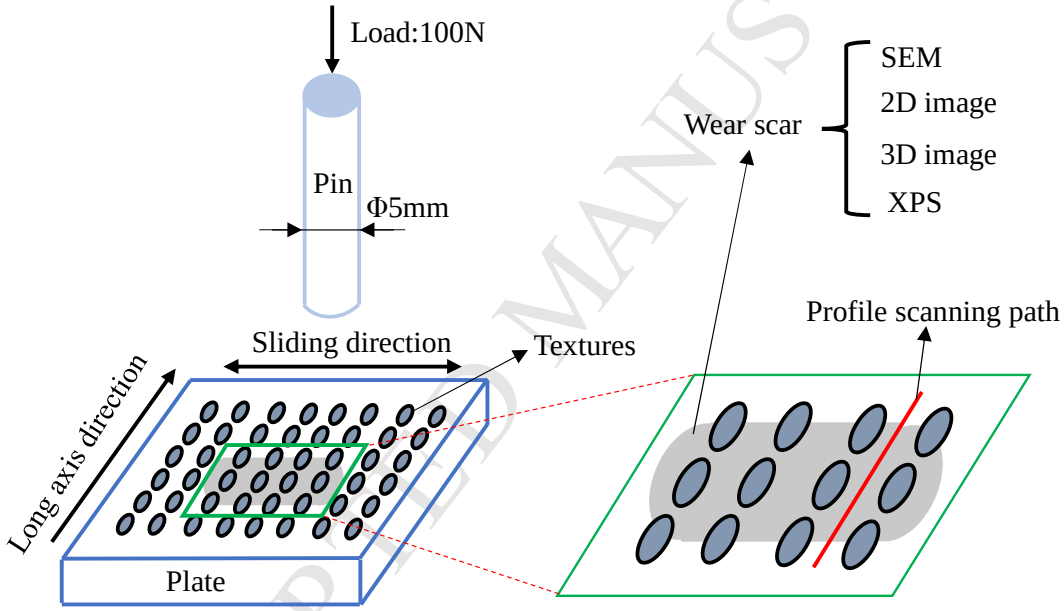

Fig. 1 Schematic of the pin-on-plate tribometer

Table 1. Tribological test conditions

Test conditions	Item or value
Lubricant	L-AN32 machine oil
Stroke length /mm	5
Testing temperature /^{o}C	25-27
Sliding velocity /mm·s^{-1}	50
Normal load /N	100

Duration /min	80

2.2 Materials

The lower specimen plate was composed of SAE1020 steel with a pristine surface roughness R_a of 0.75 μm. The upper pin specimen was made of SAE1045 steel with the diameter of 5 mm and the flat end surface roughness R_a less than 0.05 μm. The lubricant was L-AN32 machine oil obtained from Sino Petroleum Corporation, China. The main chemical components of this lubricating oil are hydrocarbons with sulfur-containing additives (concentration less than 0.5%). The basic physiochemical parameters of the L-AN32 machine oil are shown in **Table 2**.

Table 2 Physiochemical properties of the lubricating oil

Item	Value	ASTM method
Dynamic viscosity /40 °C $mm^2 \cdot s^{-1}$	32	D445
Pour point /°C	-18	D97
Mechanical impurities /%	0.007	D473
Water by distillation /%	Trace amount	D95
Flash point (open cup) /°C	220	D92
Copper strip corrosion /100 °C, 3h, grade	1	D130

2.3 Surface texturing with photolithographic etching

The protocol for forming the textured surfaces has been described in detail elsewhere [18]. Briefly, Shipley S1813 photoresist was first spun onto the surface of the SAE1020 steel plate. The coated plate was then heated at 115 °C for 2 min, covered by the lithography mask

and radiated for half an hour with ultraviolet. The processed coating was then washed by a MF-321 developer and rinsed by deionization water. After being backed, the specimen was plunged in a 3% dilute nitric acid solution for etching and then rinsed in acetone to remove the photoresist. The masks used for photolithographic patterning were printed on a laser printer with the resolution of 1200 dpi and consisted of ovals with a distance between adjacent oval centers of 2 mm. The ratios of the major to the minor axes of the ovals were designed to vary from 900/600, 1200/600 to 1800/600 μm, which are referred to as ST, MT and LT surfaces.

2.4 Surface analysis

A VK-X100 3D laser-scanning microscope (Keyence, Japan) was applied to observe the 2D and 3D optical micrographs and the surface profiles before and after sliding as well. An Thermo Scientific ESCALAB 250 X-ray photoelectron spectrometer (XPS) was used to measure the components and chemical shifts of the rubbed surfaces on the steel plate with Al Kα radiation at a power of 150 W. The spectra were collected using a pass energy of 20 eV and the components of the XPS profiles were fitted with XPSPEAK software using mixed Lorentzian-Gaussian profiles.

3. Results and discussion

3.1 Friction and wear results under full lubrication

Fig. 2 presents the optical images and profiles of the lower plate specimens before and after texturing. A smooth surface can be seen before texturing (Fig. 2a). The oval dimples

were evenly distributed over the surfaces, suggesting the successful fabrication of the textured surfaces (Figs. 2b-d).

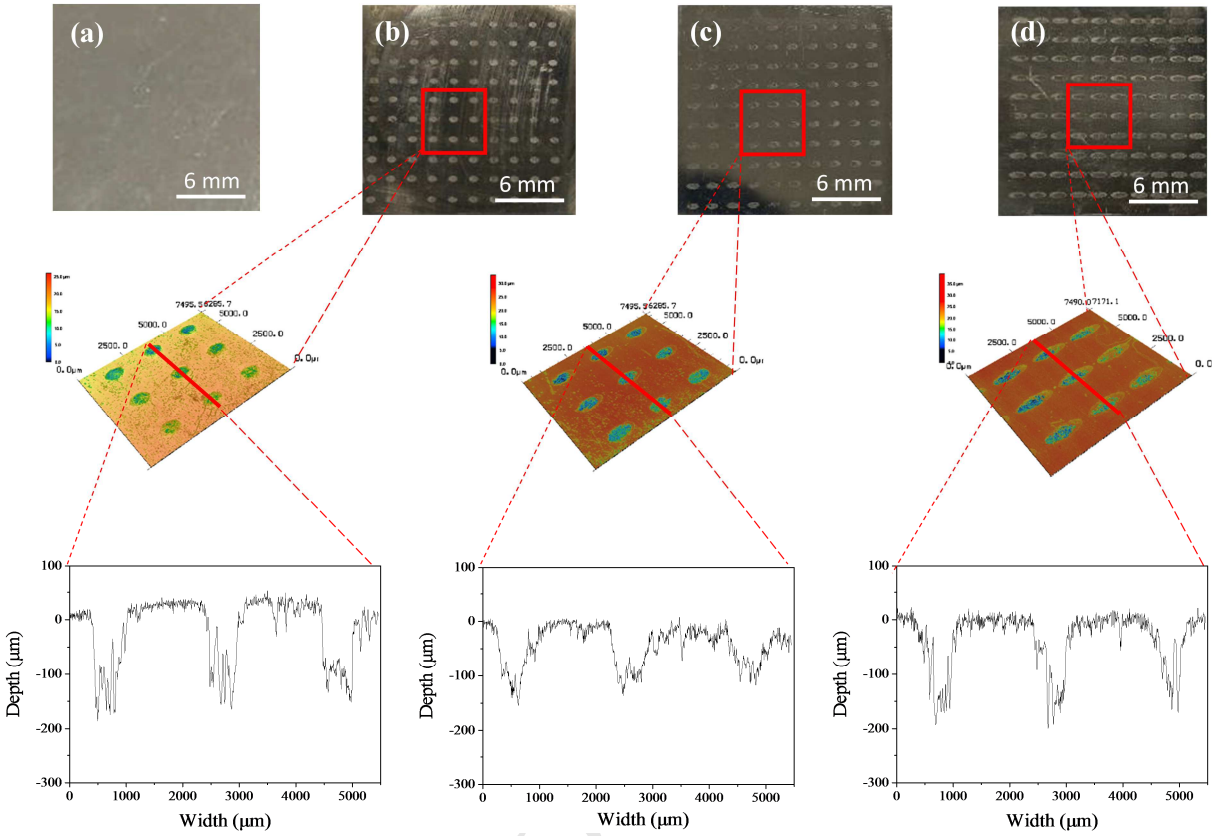

Fig. 2 Optical images and profiles of the untextured surface (UT) (a) and the textured surfaces with different ratios of the major to minor axes of the ovals (μm/μm): 900/600 (ST) (b), 1200/600 (MT) (c), and 1800/600 (LT) (d)

Fig. 3 shows the friction coefficient of the tribopairs and the wear volume of the plate under full lubrication. As can be seen, for all four surfaces, the run-in period lasted for ~35 min. At this stage, the ST and MT surfaces had a lower friction than the UT surface, while the LT surface had higher friction. Subsequently, sliding became stable, and all friction coefficients became constant, which implies the formation of similar surface films [31]. The

final wear volume of the UT surface was higher than those of the ST and MT surfaces, but lower than that of the LT surface, indicating a good antiwear performance of the ST and MT surfaces (Fig. 3b).

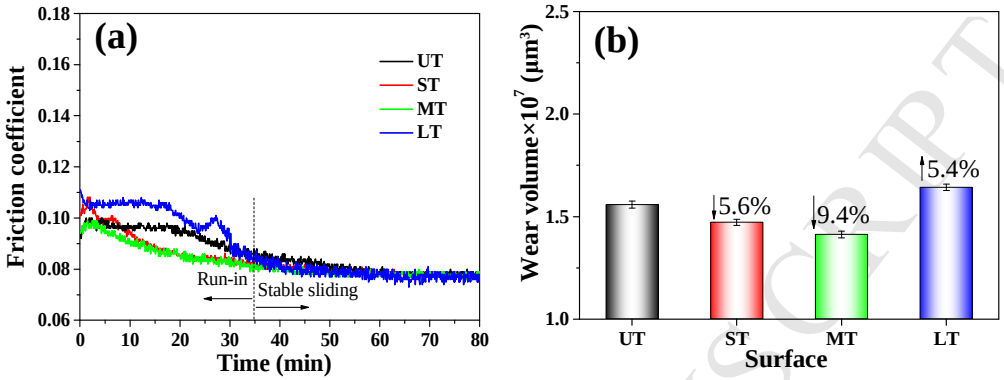

Fig. 3 The variation of friction coefficient versus sliding time (a), and wear volume of the plate (b) under fully lubricated conditions

The 2D images, surface profile curves and 3D images of the worn surfaces are presented in **Fig. 4.** The wear tracks on the worn surfaces are clearly seen for all specimens. The widths of the wear tracks are less than the pin diameter, and the cross-sectional profiles are close to parabolic. This indicates that the lubrication effects in the boundary area were better than that in the center of the rubbing surfaces. Both the widths and depths of the wear scars of the ST and MT surfaces are smaller than those of the UT surface, which agrees well with the wear results in Fig. 3b. Moreover, the boundaries of the wear tracks become vague due to the lubrication improvement of the ST and MT surfaces [32]. However, the LT surface shows a wider and deeper wear furrow than the UT surface, again matching well with the results in Fig.2b. This is consistent with the textured surfaces being able to hold more oil in the sliding interface, which is helpful for the formation of an adsorbed oil film on the ST and MT

surfaces.

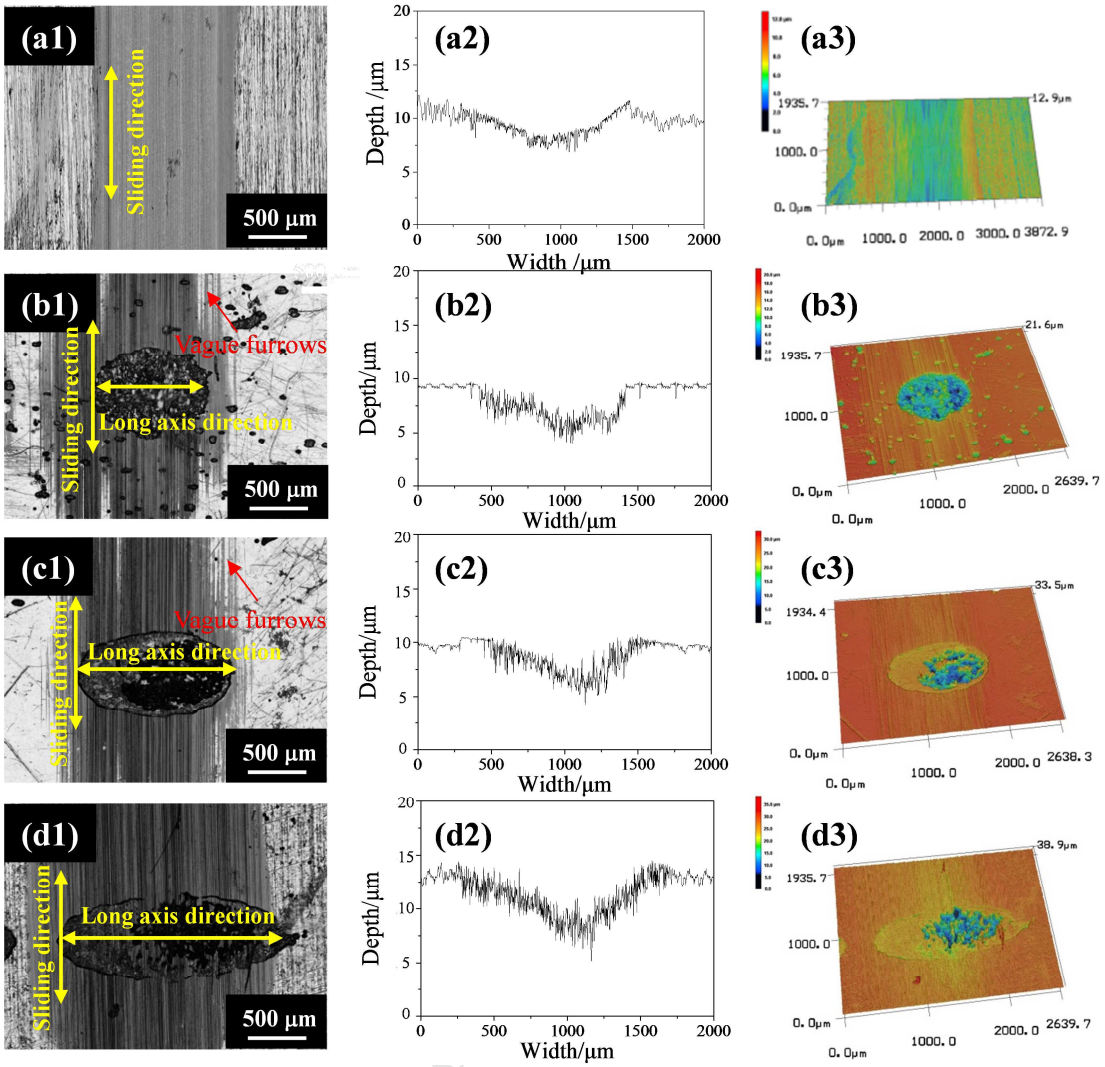

Fig. 4 2D images, surface profile curves and 3D images of worn surfaces under full lubrication: UT (a), ST (b), MT (c), and LT (d)

3.2 Friction and wear results under starved lubrication

The friction and wear results under starved lubrication conditions are shown in **Fig. 5.** As can be seen, all the specimens had higher friction and wear under starved lubrication than under full lubrication (Fig. 3). Moreover, under starved lubrication, all textured surfaces had lower friction than the UT surface. Under starved lubrication, the ST and MT surfaces show

relatively stable friction, while the friction coefficient increases monotonically with sliding time on the LT surface. The wear volumes of the ST and MT surfaces decreased by ~10 and ~23% compared to that of the UT surface. However, the wear of the LT surfaces increased significantly by ~35%, again suggesting that too large a ratio of the major to the minor axis of the oval does not provide antiwear effects. This phenomenon, LT surface having a higher wear rate, is similar to that found under full lubrication.

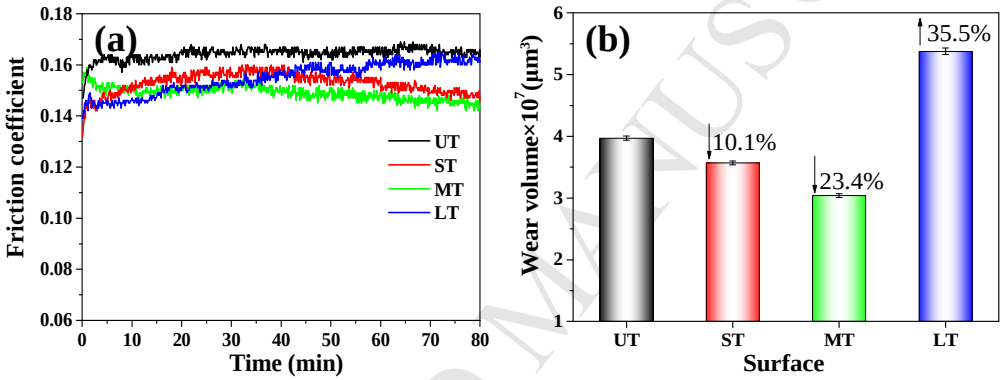

Fig. 5 The variation of friction coefficient versus sliding time (a), wear volume of the plate (b) under starved lubrication conditions

The 2D images, profile curves and 3D images of the worn surfaces under the staved lubrication are shown in **Fig. 6.** A wide and deep wear scar is found for the worn UT surface, but narrower and shallower scars were seen for the ST and MT surfaces while the LT surface had a wider and deeper wear scar. These results are consistent with the 3D images of the wear tracks. These results are also in accord with the wear results (Fig. 5b).

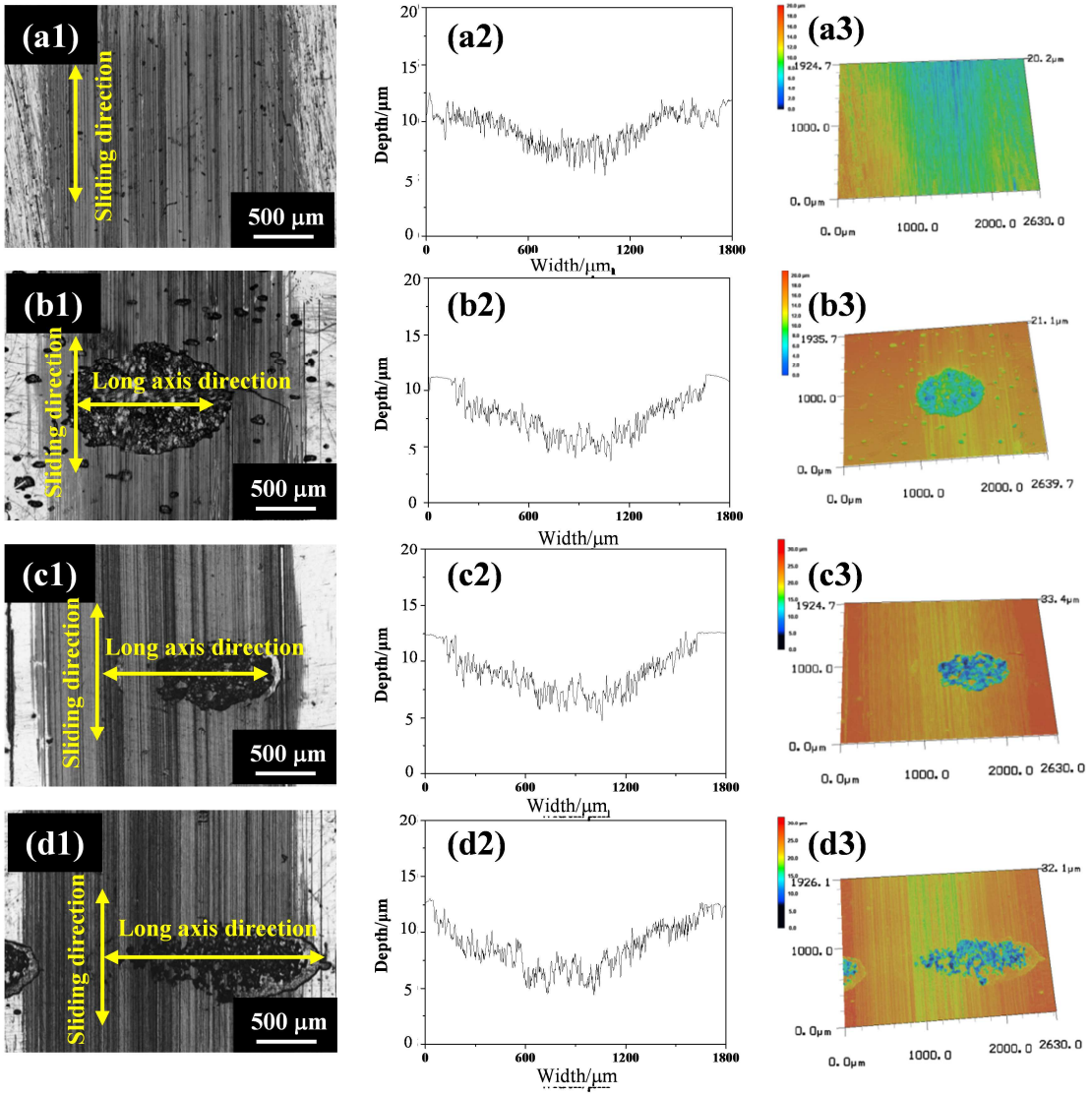

Fig. 6 2D images, surface profile curves and 3D images of worn surfaces under starved lubrication: UT (a), ST (b), MT (c), and LT (d)

3.3 XPS analyses of the worn surfaces

Although XPS analysis reflects the information from the surfaces at the nano-scale, the thicknesses of the tribofilms are usually in nano-scale range, especially under starved or boundary lubrication. In addition, XPS results can provide information on the relative concentrations of the components on the surfaces, which can represent the relative thickness of the tribofilm [33, 34]. **Table 3** shows the relative surface concentrations of the predominant

elements (Si, Mn, S, Fe and C) on the worn surfaces under different lubricating conditions measured using XPS. Si, Mn and Fe should come from the steel-plate substrate, and C, O and S are assigned to the presence of an adsorbed oil film from the base oil or a tribofilm formed from the additives. Under full lubrication, the relative coverages of carbon and oxygen were higher than those formed under the starved lubrication. This is consistent with the formation a thicker adsorbed oil film during the final stable stage of friction (Fig. 3a) [35], and the resulting better friction reduction and antiwear properties under full lubrication than those under starved lubrication. Under the same lubrication conditions, the ST and MT surfaces had a higher sulfur content than the UT and LT surfaces. This suggests that the ST and MT surfaces might form a thicker tribofilm, which contributed to the lower wear (Fig. 3b).

On the other hand, the ratio of the total areas of dimples to the area for the ST, MT and LT surfaces is 10.6%, 14.1% and 21.2%, respectively. This indicates that the contact pressure on LT surfaces was much higher than on the ST and MT surfaces. Furthermore, the highly elliptical wear scar of the LT surface can lead to a higher stress concentration, which may interfere with the formation of an adsorbed oil film [14], resulting in higher friction during the initial stage of rubbing, and a resulting higher wear rate. In addition, combining the XPS results in Table 3 and tribological behavior in Fig. 3 and Fig. 5, it can be seen that the adsorbed oil film dominated the tribological behavior under full lubrication, while the formation of a tribofilm could significantly affect sliding under starved lubrication [36].

Table 3 The content of the main elements on the worn surfaces detected by XPS under different lubrication conditions

Lubrication condition	Worn surface	Atomic percent (%)					
		Si	Mn	S	Fe	C	O
Full lubrication	UT	1.23	0.31	1.18	1.24	73.01	23.03
	ST	1.35	0.53	1.78	2.19	71.18	22.97
	MT	1.87	0.47	1.91	3.21	67.31	25.23
	LT	1.56	0.36	0.64	3.61	68.85	24.98
Starved lubrication	UT	2.11	2.13	0.66	25.83	38.15	31.12
	ST	1.28	1.19	0.89	25.63	41.55	29.46
	MT	1.93	1.45	0.98	22.11	44.57	28.96
	LT	2.03	2.36	0.47	28.87	35.67	30.6

In order to gain further insights into the lubrication mechanism, XPS spectra were collected for the main elements detected on the worn surfaces and are presented in Figs. 7 (C 1*s*), 8 (Fe 2*p*), 9 (O 1*s*) and 10 (S 2*p*). The C 1*s* spectra in **Fig. 7** can be fitted to three components at ~288.5 (peak 1), ~286.5 (peak 2), and ~284.7 (peak 3) eV binding energies, which can be assigned to the presence of COOR or carbonate species (peak 1), a carbon-hydroxyl group (peak 2) and carbon chain containing C–C(H) functionalities (peak 3) [37]. The coverage of carbon-chain containing hydrocarbons on the rubbed surfaces under full lubrication (Figs. 7a-d) are higher than those under starved lubrication (Figs. 7a'-d'), but the contents of the alcohols (with carbon-hydroxyl group) show the opposite trend. This might be due to the fact that the alcohols adsorb more easily on the sliding metal surfaces under starved lubrication because of the stronger binding of the hydroxyl groups for the H-bonding on metal surfaces [38]. In addition, the contents of esters or carbonates changed slightly under different

lubrication conditions.

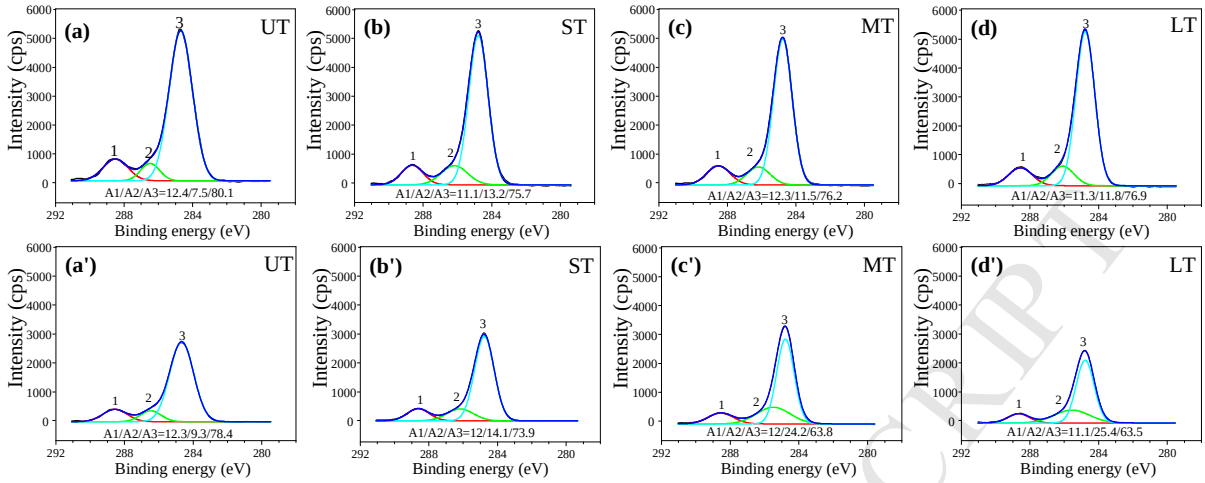

Fig. 7 C 1*s* spectra of the worn surfaces under full lubrication (a-d) and starved lubrication (a'-d'): UT (a), ST (b), MT (c), and LT (d)

Fig. 8 displays the Fe 2*p* spectra of the worn surfaces under full (Figs. 8a-d) and starved lubrication (Figs. 8a'-d'). The doublet is due the spin-orbit split Fe $2p_{1/2}$ and Fe $2p_{3/2}$ components. The Fe 2*p* profile can be fit to two components with an Fe $2p_{3/2}$ state at ~711.9 (peak 1) and 710.8 (peak 2) eV binding energies and can be ascribed to the presence of ferrous sulfide (peak 1) and iron oxide (peak 2) [39]. No Fe 2*p* in iron feature was detected at 706.7 eV indicating that the rubbed surfaces were covered by a tribofilm. The UT, ST and MT surfaces had the highest concentrations of ferrous sulfide under starved lubrication compared to that under full lubrication, indicating that starved lubrication facilitated the formation of a tribofilm. In addition, a higher coverage of ferrous sulfide was found on the ST and MT surfaces than on the UT and LT surfaces under starved conditions, which is consistent with the tribological behavior and implies that tribofilm formation controlled the friction and wear behavior during starved lubrication. In contrast, the coverage of ferrous sulfide in the wear

tracks under full lubrication did not correlate with the friction and wear behavior and might indicate that, in addition to forming a tribofilm, the adsorbed lubricant film under full lubrication contributed to the friction and wear properties [40].

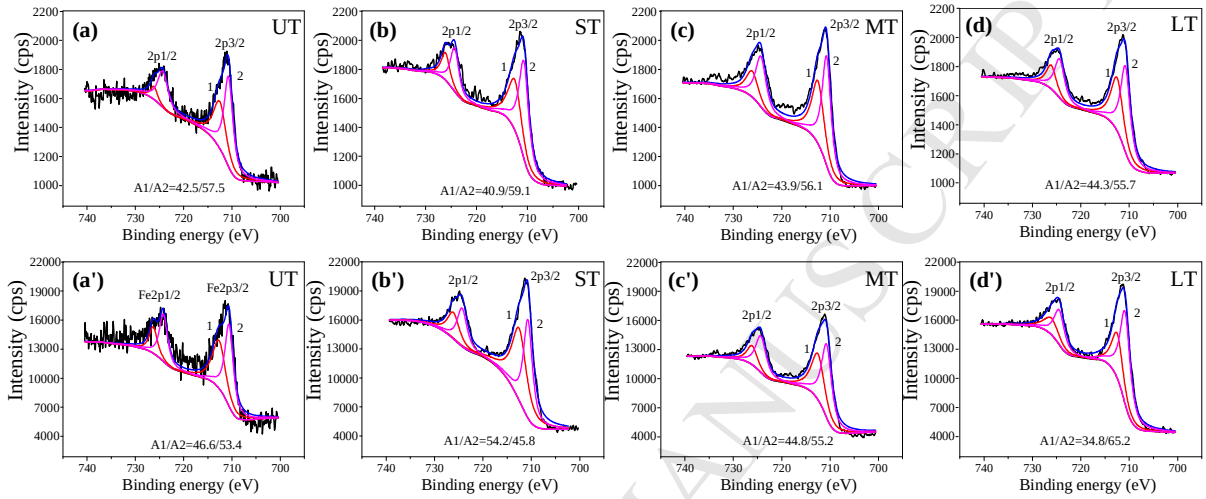

Fig. 8 Fe 2*p* spectra of the worn surfaces under full lubrication (a-d) and starved lubrication (a'-d'): UT (a), ST (b), MT (c), and LT (d)

Fig. 9 shows the O 1*s* spectra, which can be fitted to three components at ~533 (peak 1), ~531.7 (peak 2), and ~530.6 (peak 3) eV binding energies, assigned to the presence of SiO_2 (peak 1) [41], hydroxides (peak 2) and iron oxide (peak 3) [42]. It is proposed that these components derive from the substrate, adsorbed film and the tribofilm, respectively. The relative intensity of the O 1*s* components in Fig. 9 suggests that the hydroxide coverage decreased, while that of the iron oxide increased when the lubrication conditions changed from full to starved lubrication. This is also in accord with the proposal that starved lubrication aided tribofilm formation and resulted in a decrease in the thickness of the adsorbed film.

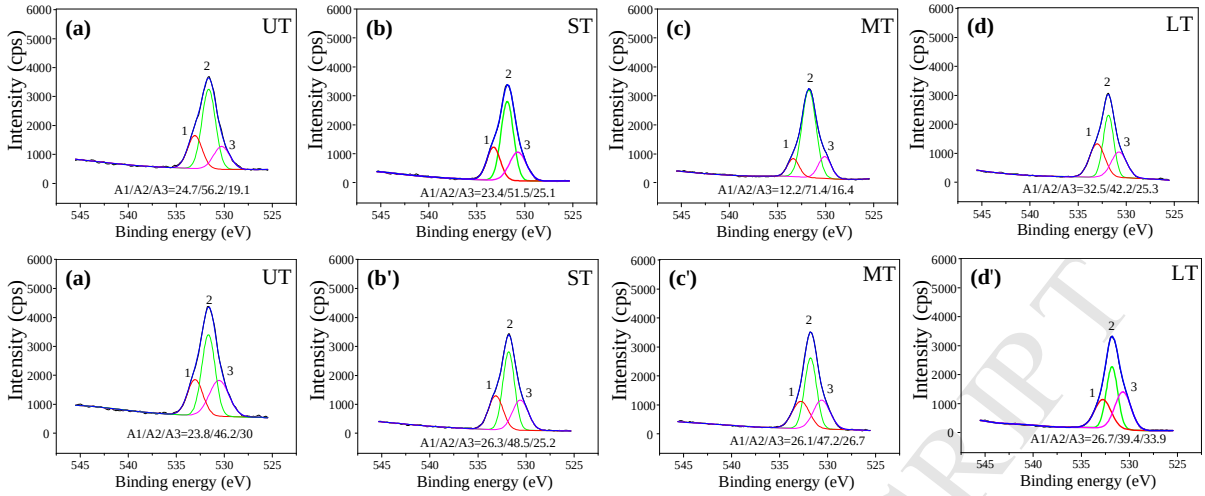

Fig. 9 O 1*s* spectra of the worn surfaces under full lubrication (a-d) and starved lubrication (a'-d'): UT (a), ST (b), MT (c), and LT (d)

The corresponding S 2*p* spectra are displayed for samples under full and starved lubrication in **Fig. 10** which have noisier profiles than for the other elements implying a relatively lower coverage of sulfur-containing species on the worn surfaces. The fitted components are at ~162.5 (peak 1), ~161.3 (peak 2) eV binding energies. These features are assigned to the overlapping spin-obit split S $2p_{1/2}$ and $2p_{3/2}$ doublets of metal sulfides [43], and is associated with an Fe 2*p* feature with a Fe $2p_{3/2}$ binding energy of ~711.9 eV (peak 1, Fig. 8). The fitted components at ~170.5 (peak 3) and ~169.3 (Peak 4) eV binding energy are assigned to the combined S $2p_{1/2}$ and $2p_{3/2}$ features of sulfates [18]. However, sulfate features are not detected in the O 1*s* (Fig. 9) or the Fe 2*p* (Fig. 8) spectra, which implies that it is present in very low concentrations. The relative higher intensity of iron sulfides on the ST and MT wear tracks under starved lubrication conditions is in accord with their lower friction, because of the laminar structure of the iron sulfides [44]. In contrast, the formation of iron sulfates as wear debris on the LT surface under full and starved lubrication and the UT surface

under starved lubrication lead to worse lubrication [18].

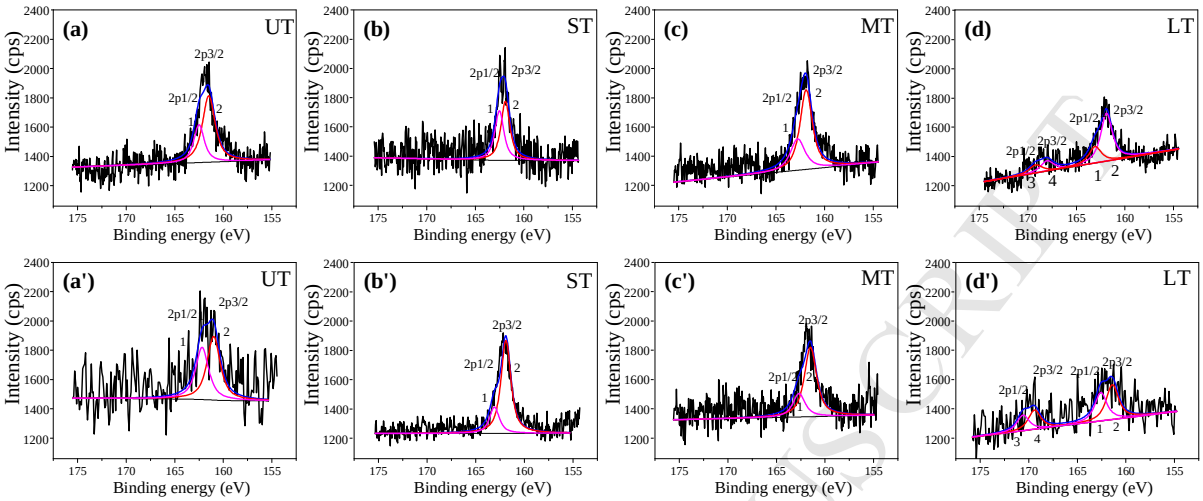

Fig. 10 S 2*p* spectra of the worn surfaces under full lubrication (a-d) and starved lubrication (a'-d'): UT (a), ST (b), MT (c), and LT (d)

The results of the surface analysis lead to the following conclusions regarding the lubrication mechanisms. Under full lubrication, the presence of an adsorbed oil film dominated the tribological behavior of the tribopairs. After completion of the run-in period, both textured and untextured surfaces reached similar friction coefficients, and the samples with ST and MT dimples had lower wear than the UT and LT surfaces. This is proposed to be due to the presence of the untextured surfaces and very high ratio of the major to minor axis of the wear scars that were deleterious to or even destroyed the adsorbed oil film.

Under starved lubrication, the formation of the tribofilm dominated the sliding process and all textured surfaces had lower coefficient than the untextured sample. In addition to the formation of lubricant micro-reservoirs and their ability to trap wear debris, the formation of the tribofilm within the wear scar significantly affected the tribological behavior. The ST and

MT surfaces had better antiwear performance than the UT surface, while the LT surfaces had worse antiwear properties, and this is proposed to be due to the fact that the excessively high ratio of the long axis to the minor axis of the oval contributed to wear debris formation and increasing wear due to the destruction of the tribofilm by high contact stresses. The appropriate ST and MT surfaces helped the formation of a tribofilm containing lubricious metal sulfides, which accounted for their good tribological performances.

4. Conclusions

The tribological behavior of the textured surfaces with oval shapes by chemical etching was investigated on a pin-on-plate tribometer. The formation of the tribofilm was studied under full and starved lubrication. It was found that the friction coefficient and wear loss of the tribopairs under full lubrication were lower than those under starved lubrication for both textured and untextured surfaces, suggesting that the lubrication regime played a more important role than surface texture.

Under full lubrication, at the stable stage, the friction coefficient was similar for all the textured and untextured steel/steel surfaces since they were dominated by the adsorbed oil film. Under starved lubrication, the formation of tribofilm including slippery iron sulfide was responsible for the lower friction and wear of the ST and MT surfaces.

The excessively high ratio of the long axis to the minor axis of the oval can enhance the contact stress and destroy the tribofilm resulting in formation of wear debris, which was deleterious to the lubrication. Besides the micro-reservoirs of lubricating oil and wear debris trapping roles, the formation of the tribofilm on the textured surfaces should be considered

since it can significantly affect friction and wear properties.

Acknowledgements:

This work is supported by the National Natural Science Foundation of China (Grant No. 51875155) and the Fundamental Research Funds for the Central Universities. We acknowledge Prof. Kunhong Hu, Dr. Enzhu Hu and Mr Jian Geng for their help with the tribo-tests.

References:

[1] Arenas M, Ahuir-Torres J, García I, Carvajal H, de Damborenea J. Tribological behaviour of laser textured Ti6Al4V alloy coated with MoS_2 and graphene. Tribol Int 2018;128:240-7.

[2] Etsion I. State of the art in laser surface texturing. Journal of tribology 2005;127:248-53.

[3] Cunha A, Elie A-M, Plawinski L, Serro AP, do Rego AMB, Almeida A, et al. Femtosecond laser surface texturing of titanium as a method to reduce the adhesion of Staphylococcus aureus and biofilm formation. Appl Surf Sci 2016;360:485-93.

[4] Taee M, Torabi A, Akbarzadeh S, Khonsari MM, Badrossamay M. On the performance of EHL contacts with textured surfaces. Tribol Lett 2017;65:85.

[5] Li J, Liu S, Yu A, Xiang S. Effect of laser surface texture on CuSn6 bronze sliding against PTFE material under dry friction. Tribol Int 2018;118:37-45.

[6] Vlădescu S-C, Medina S, Olver AV, Pegg IG, Reddyhoff T. Lubricant film thickness and friction force measurements in a laser surface textured reciprocating line contact simulating the piston ring–liner pairing. Tribol Int 2016;98:317-29.

[7] Wakuda M, Yamauchi Y, Kanzaki S, Yasuda Y. Effect of surface texturing on friction reduction between ceramic and steel materials under lubricated sliding contact. Wear 2003;254:356-63.

[8] Arslan A, Masjuki H, Kalam M, Varman M, Mufti R, Mosarof M, et al. Surface texture manufacturing techniques and tribological effect of surface texturing on cutting tool performance: a review. Crit Rev Solid State Mater Sci 2016;41:447-81.

[9] Chen L, Liu Z, Shen Q. Enhancing tribological performance by anodizing micro-textured surfaces with nano-MoS2 coatings prepared on aluminum-silicon alloys. Tribol Int 2018;122:84-95.

[10] Liu D, Wu Z, Yan B, Shen B, Liu L, Hu W. Tribological performances of textured surfaces prepared by electrodeposition method. Surf Eng 2017;33:877-85.

[11] Li X, Li Y, Tong Z, Ma Q, Ni Y, Dong G. Enhanced lubrication effect of gallium-based liquid metal with laser textured surface. Tribol Int 2019;129:407-15.

[12] Grabon W, Pawlus P, Wos S, Koszela W, Wieczorowski M. Effects of honed cylinder liner surface texture on tribological properties of piston ring-liner assembly in short time tests. Tribol Int 2017;113:137-48.

[13] Sedlaček M, Podgornik B, Ramalho A, Česnik D. Influence of geometry and the sequence of surface texturing process on tribological properties. Tribol Int 2017;115:268-73.

[14] Olofinjana B, Lorenzo-Martin C, Ajayi OO, Ajayi EO. Effect of laser surface texturing (LST) on tribochemical films dynamics and friction and wear performance. Wear 2015;332-333:1225-30.

[15] Kovalchenko A, Erdemir A, Ajayi O, Etsion I. Tribological behavior of oil-lubricated

laser textured steel surfaces in conformal flat and non-conformal contacts. Mater Perform Char 2017;6:1-23.

[16] Mishra P, Ramkumar P. Effect of micro texture on tribological performance of piston ring-cylinder liner system under different lubrication regimes. SAE Technical Paper; 2018-28-0052.

[17] Grabon W, Koszela W, Pawlus P, Ochwat S. Improving tribological behaviour of piston ring–cylinder liner frictional pair by liner surface texturing. Tribol Int 2013;61:102-8.

[18] Xu Y, Yu J, Geng J, Abuflaha R, Olson D, Hu X, et al. Characterization of the tribological behavior of the textured steel surfaces fabricated by photolithographic etching. Tribol Lett 2018;66:55.

[19] Equey S, Roos S, Mueller U, Hauert R, Spencer ND, Crockett R. Tribofilm formation from ZnDTP on diamond-like carbon. Wear 2008;264:316-21.

[20] Morina A, Neville A. Understanding the composition and low friction tribofilm formation/removal in boundary lubrication. Tribol Int 2007;40:1696-704.

[21] Komvopoulos K, Chiaro V, Pakter B, Yamaguchi E, Ryason P. Antiwear tribofilm formation on steel surfaces lubricated with gear oil containing borate, phosphorus, and sulfur additives. Tribol T 2002;45:568-75.

[22] Qiu M, Minson BR, Raeymaekers B. The effect of texture shape on the friction coefficient and stiffness of gas-lubricated parallel slider bearings. Tribol Int 2013;67:278-88.

[23] Yu H, Wang X, Fei Z. Geometric shape effects of surface texture on the generation of hydrodynamic pressure between conformal contacting surfaces. Tribol Lett 2010;37:123-30.

[24] Pettersson U, Jacobson S. Influence of surface texture on boundary lubricated sliding

contacts. Tribol Int 2003;36:857-64.

[25] Zhang P, Chen H, Zhang L, Zhang D. Anti-adhesion effects of liquid-infused textured surfaces on high-temperature stainless steel for soft tissue. Appl Surf Sci 2016;385:249-56.

[26] Zhang H, Ding B, Chen T. A high efficiency industrial polysilicon solar cell with a honeycomb-like surface fabricated by wet etching using a photoresist mask. Appl Surf Sci 2016;387:1265-73.

[27] Lewis R, Carré MJ, Abu Bakar A, Tomlinson SE. Effect of surface texture, moisture and wear on handling of rugby balls. Tribol Int 2013;63:196-203.

[28] Li X, Sosa M, Olofsson U. A pin-on-disc study of the tribology characteristics of sintered versus standard steel gear materials. Wear 2015;340-341:31-40.

[29] Wang W, Liu K, Jiao M. Thermal and non-Newtonian analysis on mixed liquid–solid lubrication. Tribol Int 2007;40:1067-74.

[30] Kovalchenko A, Ajayi O, Erdemir A, Fenske G, Etsion I. The effect of laser texturing of steel surfaces and speed-load parameters on the transition of lubrication regime from boundary to hydrodynamic. Tribol T 2004;47:299-307.

[31] Zeng X, Li J, Wu X, Ren T, Liu W. The tribological behaviors of hydroxyl-containing dithiocarbamate-triazine derivatives as additives in rapeseed oil. Tribol Int 2007;40:560-6.

[32] Sato O, Takiguchi M, Takayuki A, Seki Y, Fujimura K, Tateishi Y. Improvement of piston lubrication in a diesel engine by means of cylinder surface roughness. SAE technical paper; 2004-01-0604.

[33] Heuberger R, Rossi A, Spencer ND. XPS study of the influence of temperature on ZnDTP tribofilm composition. Tribol Lett 2007;25:185-96.

[34] Engqvist H, Högberg H, Botton GA, Ederyd S, Axén N. Tribofilm formation on cemented carbides in dry sliding conformal contact. Wear 2000;239:219-28.

[35] Spikes H. Friction modifier additives. Tribol Lett 2015;60:5.

[36] Saeidi F, Parlinska-Wojtan M, Hoffmann P, Wasmer K. Effects of laser surface texturing on the wear and failure mechanism of grey cast iron reciprocating against steel under starved lubrication conditions. Wear 2017;386-387:29-38.

[37] Xu Y, Peng Y, Dearn KD, You T, Geng J, Hu X. Fabrication and tribological characterization of laser textured boron cast iron surfaces. Surf Coat Technol 2017;313:391-401.

[38] Song JY, Jhung SH. Adsorption of pharmaceuticals and personal care products over metal-organic frameworks functionalized with hydroxyl groups: Quantitative analyses of H-bonding in adsorption. Chem Eng J 2017;322:366-74.

[39] Ferris F, Tazaki K, Fyfe W. Iron oxides in acid mine drainage environments and their association with bacteria. Chem Geol 1989;74:321-30.

[40] Peng DX, Kang Y, Hwang RM, Shyr SS, Chang YP. Tribological properties of diamond and SiO_2 nanoparticles added in paraffin. Tribol Int 2009;42:911-7.

[41] Pan T-M, Huang C-C. Effects of oxygen content and postdeposition annealing on the physical and electrical properties of thin Sm_2O_3 gate dielectrics. Appl Surf Sci 2010;256:7186-93.

[42] Bhattacharya P, Nandasiri MI, Lv D, Schwarz AM, Darsell JT, Henderson WA, et al. Polyamidoamine dendrimer-based binders for high-loading lithium–sulfur battery cathodes. Nano Energy 2016;19:176-86.

[43] Zhu Y, Li Z, Chen M, Cooper HM, Lu GQM, Xu ZP. One-pot preparation of highly fluorescent cadmium telluride/cadmium sulfide quantum dots under neutral-pH condition for biological applications. J Colloid Interface Sci 2013;390:3-10.

[44] De Barros M-I, Bouchet J, Raoult I, Le Mogne T, Martin J-M, Kasrai M, et al. Friction reduction by metal sulfides in boundary lubrication studied by XPS and XANES analyses. Wear 2003;254:863-70.

Highlights

- Textured surfaces with oval-shaped dimples were facilely fabricated.
- Influence of tribofilm formation on the surface tribological behavior was investigated.
- The adsorbed-film controlled the friction and wear behavior of tribo-pairs under full lubrication.
- The formation of tribofilm dominated the interface behavior under starved lubrication.